Laguerre-Gaussian modes in a double-end-pumped microchip laser: superposition and competition

2001 J. Opt. B: Quantum Semiclass. Opt. 3 146

(http://iopscience.iop.org/1464-4266/3/3/312)

INSTITUTE OF PHYSICS PUBLISHING JOURNAL OF OPTICS B: QUANTUM AND SEMICLASSICAL OPTICS

J. Opt. B: Quantum Semiclass. Opt. **3** (2001) 146–151 www.iop.org/Journals/ob PII: S1464-4266(01)20196-7

Laguerre–Gaussian modes in a double-end-pumped microchip laser: superposition and competition

Y F Chen[1,3] **and Y P Lan**[2]

[1] Department of Electrophysics, National Chiao Tung University, 1001 T A Hsueh Road, Hsinchu, Taiwan 30050, People's Republic of China
[2] Institute of Electro-Optical Engineering, National Chiao Tung University, 1001 T A Hsueh Road, Hsinchu, Taiwan 30050, People's Republic of China

E-mail: yfchen@cc.nctu.edu.tw

Received 18 December 2000, in final form 8 March 2001

Abstract
A double-end-pumped microchip laser is developed to investigate the superposition and competition of the Laguerre–Gassian (LG) modes. It is found that two LG modes can be directly superposed when the excited regions are well separated. Conversely, when the inversion populations have a considerable overlap, strong competition occurs between LG modes. The experimental result is generally consistent with the theoretical prediction for cylindrically symmetric class B lasers.

Keywords: Microchip laser, Laguerre–Gaussian mode, mode competition

The recent rapid progress of diode-pumped microchip lasers has driven a renaissance of solid-state laser physics research and led to novel phenomena [1]. Fibre delivery of the pump power enables us to keep the laser resonator separate from the pump source, so that the laser resonator can be isolated from disturbances caused by the pumping and cooling systems of the pump source. In previous works, the high-order Hermite–Gaussian modes have been systematically generated by a fibre-coupled diode end-pumped Nd:YAG laser [2, 3]. The high-order Laguerre–Gaussian (LG) $\mathrm{TEM}_{p,l}$ mode where p and l are the radial and azimuthal indices of the LG mode exhibits interesting physics [4]. Recently, we developed a technique for the generation of the cylindrical symmetry LG modes with $p = 0$ and specified values of l in a fibre-coupled diode end-pumped solid-state laser [5]. The key novelty is to produce a doughnut-shaped pump-profile by defocusing a standard fibre-coupled diode. The experimental results demonstrate that the stable transverse-mode pattern near the pump threshold is usually an LG $\mathrm{TEM}_{0,l}$ mode with the distribution $\cos^2 l\phi$ (or $\sin^2 l\phi$) in azimuthal angle, having $2l$ nodes in the azimuth. Even though the geometry is of cylindrical symmetry, there is still a certain astigmatism in the cavity due to the thermal lensing effect and anisotropic properties of the gain medium. This is the reason why sine or cosine LG modes instead of doughnut modes were generated near the pump threshold. A similar high-order LG $\mathrm{TEM}_{0,l}$ mode has been reported in electrically pumped [6] and optically pumped [7] vertical-cavity surface-emitting semiconductor lasers (VCSELs). However, the main difficulty of the emission of high-order LG modes in VCSELs is that the processed wafer is in need of extraordinary homogeneity.

In this paper, we extend the previous set-up to study the interaction of LG modes with a double-end-pumping configuration. Experimental results show that when two pumped regions are well separated, the pattern formation is the superposition of the original characteristic modes. In contrast, when there is a significant overlap between two pumped regions, transverse mode competition complicates pattern formation and results in temporal instabilities and chaotic emission.

Figure 1 shows a schematic diagram of a double-end-pumped Nd:YVO_4 laser considered in this paper. We used a plano-concave cavity that consists of one planar Nd:YVO_4 surface, high-reflection coated at 1064 nm and high-transmission coated at 809 nm for the pump light to enter the laser crystal, and a spherical output mirror. The second surface of the Nd:YVO_4 crystal (1 mm length) is anti-reflection coated at 1064 nm. A mirror with the reflectance of $R = 97.5\%$ and the radius of curvature of 250 mm was used in the resonator to couple the output power. For a 5 mm resonator length, the radius of the fundamental mode was around 0.11 mm. The transverse mode separation is of the order of 0.05 mm. The

[3] Corresponding author.

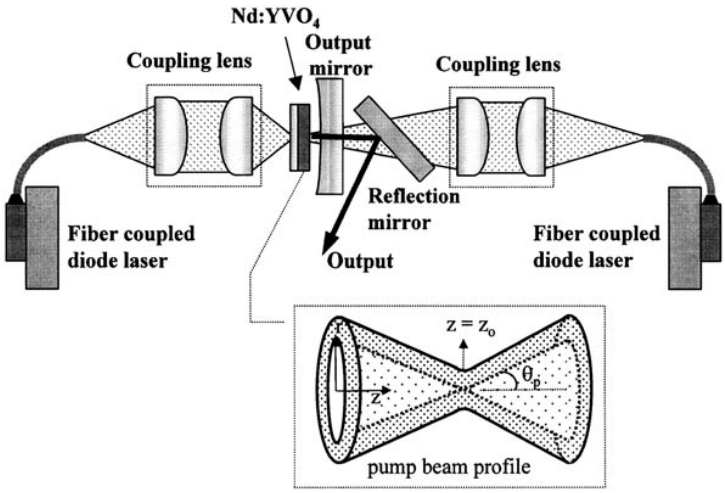

Figure 1. Schematic of a fibre-coupled diode double-end-pumped laser; a typical beam profile of a fibre-coupled laser diode away from the focal plane.

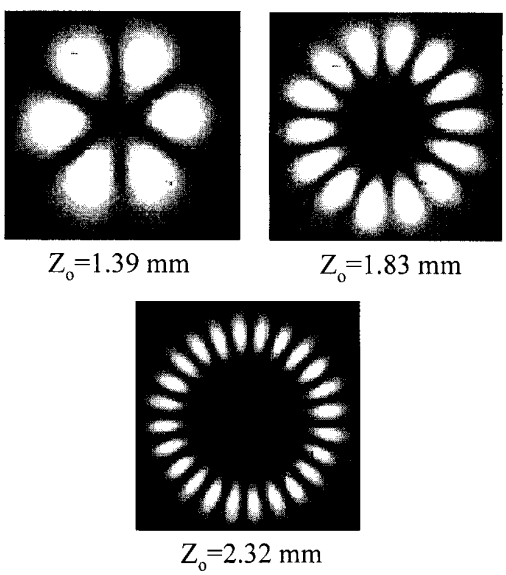

Figure 2. Beam profiles with different LG $TEM_{0,l}$ mode distributions, measured with the CCD camera, in the three positions.

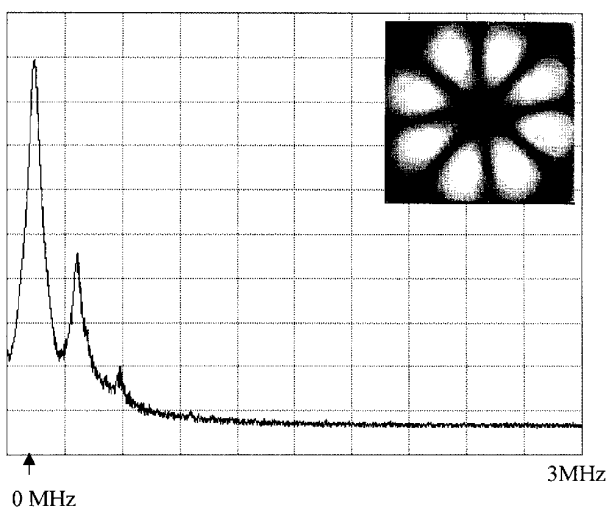

Figure 3. Power intensity spectrum of laser emission for LG $TEM_{0,4}$ mode. Vertical scale, 10 dB/div; horizontal scale, 300 kHz/div.

pump power consists of two 1 W fibre-coupled laser diodes (Coherent, F-81-800C-100) with a 0.1 mm core diameter and was focused into the Nd:YVO_4 crystal by using a focusing lens with 0.57 magnification. The thermal lensing is not significant in the experiment because the thermal power density is less than 0.5 W mm^{-2}.

For a multi-mode fibre-coupled diode laser passing through a focusing lens, the profile at the focal plane is like a top-hat distribution; however, away from the focal plane it may be like a doughnut-shaped distribution, as depicted in the inset of figure 1. With this property, we can use a single-end-pumping configuration to generate the high-order LG $TEM_{0,l}$ mode purely by defocusing a standard fibre-coupled diode. From the characteristics of the pump beam profile, the radius of maximum pump intensity amplitude can be approximately described by $r_p(z) = \theta_p|z - z_o|$, where θ_p is the far-field half-angle, the point $z = 0$ is taken to be at the incident surface of the gain medium, and z_o is the focal position of the pump beam in the laser crystal. The average radius of maximum pump intensity inside the gain medium, r_{pa}, is calculated by $\int_0^L r_p(z)\,e^{-\alpha z}\,dz \big/ \int_0^L e^{-\alpha z}\,dz$, where α is the absorption coefficient at the pump wavelength and L is the length of the laser crystal. Carrying out the integration and using $e^{-\alpha L} \to 0$, the average radius of maximum pump intensity is given by $r_{pa} = \theta_p\left[z_o + \left(2e^{-\alpha z_o} - 1\right)/\alpha\right]$.

For a single LG $TEM_{0,l}$ mode, the normalized cavity mode distribution is given by

$$s_{0,l}(r,\phi,z) = \frac{4}{(1+\delta_{0,l})\,l\,!\,\pi\,\omega_o^2 L}\left(\cos^2 l\phi\right)\left(\frac{2r^2}{\omega_o^2}\right)^l \times \exp\left(-\frac{2r^2}{\omega_o^2}\right), \quad (1)$$

where the z-dependent variation in $s_{0,l}(r,\phi,z)$ is neglected and the spot radius of the laser beam ω_o is approximated to be constant along the laser axis in the laser crystal. From equation (1), the radius of maximum mode intensity amplitude is trivially $r_{0,l} = \omega_o\sqrt{l/2}$. Since the cavity mode with

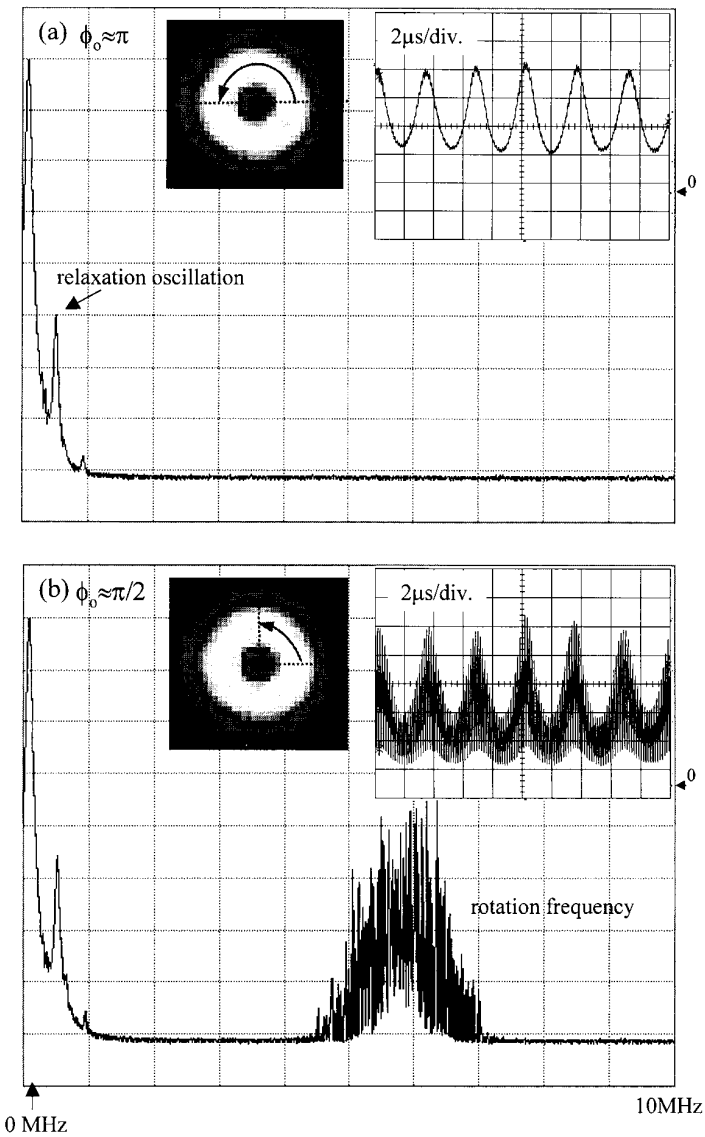

Figure 4. Spectrum recorded when the laser simultaneously oscillates in the two first-order transverse modes, (*a*) $\phi_o = \pi$ and (*b*) $\phi_o = \pi/2$ showing the rotation frequency. Vertical scale, 10 dB/div; horizontal scale, 1 MHz/div.

the biggest overlap with the gain structure has the minimum threshold, we can obtain LG $TEM_{0,l}$ mode output in a single-end-pumping configuration by adjusting the focal position z_o to achieve $r_{pa} = r_{0,l}$ for the best overlap. Figure 2 shows the experimental results for the output beam profiles with different transverse-mode distributions, measured with the CCD camera (Coherent, Beam-Code), in the three positions. The relation between transverse modes and pump positions is consistent with the prediction of pump-to-mode matching. Note that the Nd-doped lasers are class B lasers; therefore the free-running one-mode laser displays relaxation oscillations [8], as shown in figure 3.

Slightly above the pump threshold in our laser set-up, an LG $TEM^*_{0,l}$ or $TEM^*_{0,-l}$ mode, having a circle of constant intensity in the radial direction, can be generated by the superposition of two like-$TEM_{0,l}$ modes, one rotated by $\pi/2$ about the optical axis relative to the other. Since astigmatism lifts the degeneracy of the two like-LG $TEM_{0,l}$ modes, a perfectly circular pattern is usually an 'unlocked doughnut'. A nonlinear system of the Maxwell–Bloch equations in terms of partial derivatives is often reduced to a system of ordinary differential equations by expanding in terms of the empty-cavity modes for the laser system with a small number of excited transverse modes [9–12]. For class B lasers, the approximation of $\gamma_\perp \gg \kappa, \gamma_\parallel$ is usually used to simplify the system of equations where $\gamma_\perp, \kappa, \gamma_\parallel$ are the decay constants of the polarization, of the electromagnetic field and of the population inversion, respectively. In this paper, we use the system of equations derived in [12] to analyse the dynamics of the two LG $TEM_{0,l}$ modes in a class B laser. It is found that when the frequency difference between the LG $TEM_{0,l}$ cosine and sine modes considerably exceeds the relaxation frequency, the intensity distribution in a transverse section of a $TEM_{0,l}$ mode can be given by

$$I(\rho, \phi, t) = \frac{1}{l!}\rho^{2l} \exp\left(-\rho^2\right) g_l(\phi, t), \qquad (2)$$

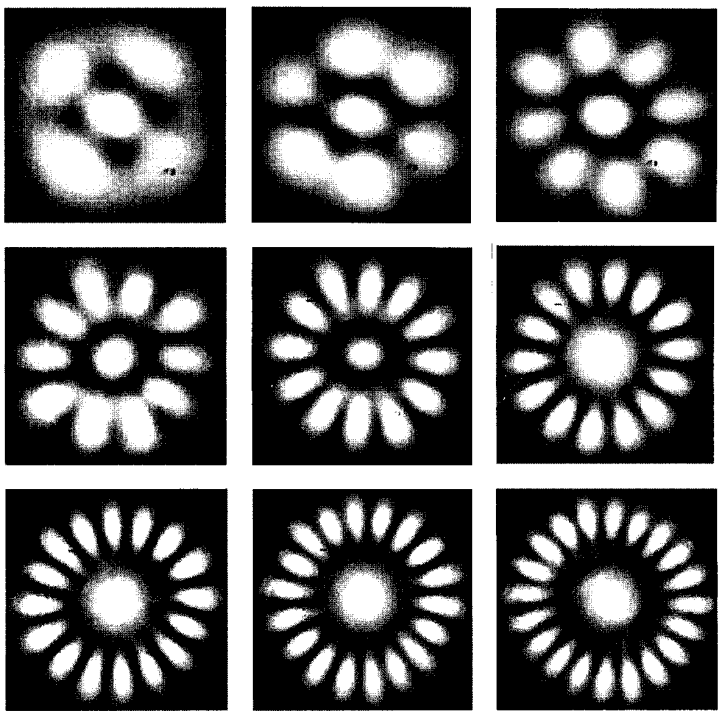

Figure 5. A sequence of output beam profiles of LG $TEM_{0,1} + TEM_{0,0}$ modes for $l = 2$–10 measured with the CCD camera.

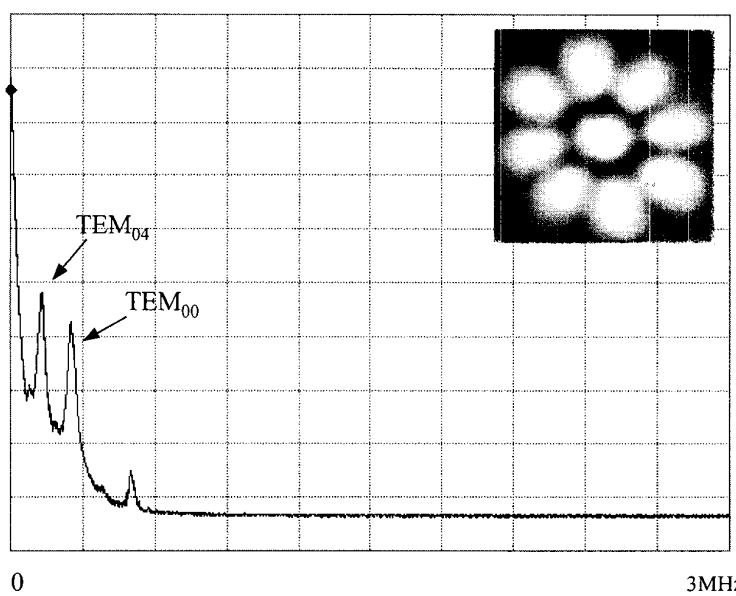

Figure 6. Power intensity spectrum of laser emission for LG $TEM_{0,4} + TEM_{0,0}$ mode. Vertical scale, 10 dB/div; horizontal scale, 300 kHz/div.

where

$$g_l(\phi, t) = |F_+|^2 + |F_-|^2 + 2\,|F_+|\,|F_-|\cos(2\,l\phi - \Omega\,t), \quad (3)$$

Ω is the frequency difference between the LG $TEM_{0,l}$ cosine and sine modes, $\rho = \sqrt{2}r/\omega_o$; ϕ is the azimuthal angle and $F_\pm \rho^l \exp\lfloor \pm i l\phi - (\rho^2/2)\rfloor$ are the amplitudes of the $TEM^*_{0,\pm l}$. Furthermore, the calculation results also show that the intensities $|F_+|^2$ and $|F_-|^2$ are in phase at the relaxation frequency and the total intensity $|F_+|^2 + |F_-|^2$ exhibits pure relaxation oscillations. For a given value of ρ, the above intensity $I(\rho, \phi, t)$ has a minimum at

$$\phi = \phi_{\min} = (\Omega\,t \pm \pi)/2\,l. \quad (4)$$

As a result, the angular velocity of rotation of the intensity minimum is $\mathrm{d}\phi_{\min}/\mathrm{d}t = \Omega/2l$. Since the pattern for the $TEM_{0,l}$ mode is invariant under rotations of π/l, the actual rotation frequency for the intensity pattern is Ω. This is the reason why the frequency difference between the LG $TEM_{0,l}$ cosine and sine modes can be interpreted as the rotation frequency of the unlocked doughnut mode [12, 13].

Previously, Boscolo *et al* [13] verified the rotation dynamics of family $q = 2$ in a CO_2 laser by using two detectors placed in different azimuthal positions to observe the phase variation. However, the measurement method of Boscolo *et al* [13] suffers a low single-to-noise ratio for the present laser system. Here we use the cumulative intensity to demonstrate the rotation dynamics of the $TEM^*_{0,\pm l}$ mode. With equation (3), the cumulative intensity is defined as

$$G_l(\phi_o, t) = \int_0^{\phi_o} g_l(\phi, t)\,\mathrm{d}\phi$$
$$= \phi_o\left(|F_+|^2 + |F_-|^2\right) + \frac{1}{l}|F_+||F_-|$$
$$\times[\sin(2l\phi_o - \Omega t) + \sin(\Omega t)], \qquad (5)$$

where ϕ_o represents the acceptance angle of the detector. Since $|F_+|^2$ and $|F_-|^2$ are in phase at the relaxation frequency, the magnitude of the component with the rotation frequency in the cumulative intensity depends on the factor $[\sin(2l\phi_o - \Omega t) + \sin(\Omega t)]$. It is easily found that if the acceptance angle is an integral multiple of π/l, the component with the rotation frequency disappears and the cumulative intensity exhibits pure relaxation oscillations. On the other hand, if the acceptance angle is an odd multiple of $\pi/(2l)$, the cumulative intensity exhibits relaxation oscillations modulated at the rotation frequency. To confirm the theoretical prediction, we use a single detector to measure the power intensity with different acceptance angles for the $TEM^*_{0,\pm l}$ mode with $l = 1$. Figures 4(*a*) and (*b*) show the experimental results of the power intensity spectra and the time characteristics for $\phi_o = \pi$ and $\pi/2$, respectively. It can be found that the experimental results agree very well with the theoretical predictions. The agreement unambiguously proves that the observed doughnut pattern is periodic in the azimuthal direction and it rotates at the measured modulation frequency. Moreover, a dynamical behaviour similar to that of the $TEM^*_{0,\pm 1}$ mode is also found for other higher $TEM^*_{0,\pm l}$ modes.

With the double-end-pumping configuration, we can study the interaction between two LG modes. The double-end-pumping method appears to be fruitful since one can adjust modal gain and the coupling strength for competing modes quite selectively. We anticipate that the potential advantages go beyond the analysis of the interaction between transverse modes of different families known so far [9–11]. Firstly, we generate the LG $TEM_{0,1} + TEM_{0,0}$ modes by using one pump source to produce the $TEM_{0,l}$ mode and using the other pump source to generate the $TEM_{0,0}$ mode. In the present experiment, the frequency difference between consecutive transverse modes is 1.36 GHz, while the frequency spacing between consecutive longitudinal modes is about 30 GHz. The present LG $TEM_{0,1} + TEM_{0,0}$ modes can be operated in a single longitudinal mode at least tenfold above threshold before the second longitudinal mode reaches threshold because the microchip gain medium has a short absorption depth that reduces the spatial hole burning effect. Figure 5 shows the experimental results for a sequence of output beam profiles of LG $TEM_{0,1} + TEM_{0,0}$ modes. Essentially, the output profiles of LG $TEM_{0,1} + TEM_{0,0}$ modes are well superposed for $l > 3$. The flower-like profiles, however, are substantially distorted in the LG $TEM_{0,2} + TEM_{0,0}$ mode and the LG $TEM_{0,3} + TEM_{0,0}$ mode since the inversion populations of the

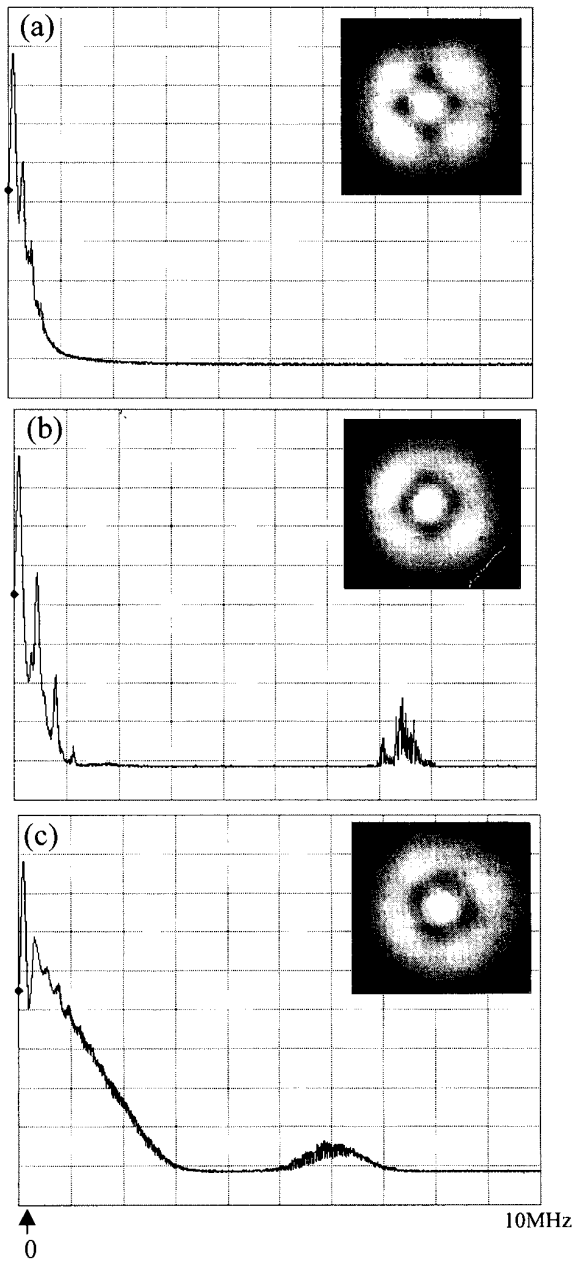

Figure 7. (*a*)–(*c*) Power spectra and the pattern formations obtained from the combination of the LG $TEM_{0,2}$ and TEM $_{0,0}$ modes. Vertical scale, 10 dB/div; horizontal scale, 1 MHz/div.

two pump regions have considerable overlapping. Figure 6 shows the experimental result for the power intensity spectrum of the LG $TEM_{0,4} + TEM_{0,0}$ mode. It can be seen that the two modes have their own relaxation frequencies. Experimental results reveal that both modes run independently without any visible phase correlation in LG $TEM_{0,1} + TEM_{0,0}$ modes for $l > 3$. Moreover, no frequency pulling effects are found. To quantify the interaction strength between $TEM_{0,0}$ and $TEM_{0,l}$ modes, we use the mode overlapping coefficient

$$C_{0,l} = \left(\pi\omega_o^2 L\right) \int s_{0,0}(r, \phi, z)\, s_{0,l}(r, \phi, z)\,\mathrm{d}V. \qquad (6)$$

Substituting equation (1) into (6), we obtain $C_{0,l} = 2^{-l}$. Therefore, it may be concluded that the complex amplitudes

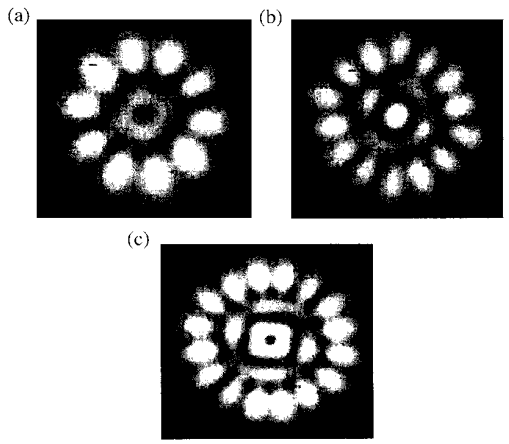

Figure 8. Experimental result for output beam profiles of multiringed LG modes, measured with the CCD camera. (*a*) $TEM^{*}_{0,\pm1} + TEM_{0,5}$, (*b*) $TEM_{0,0} + TEM^{*}_{0,\pm3} + TEM_{0,7}$ and (*c*) $TEM^{*}_{0,\pm2} + TEM^{*}_{0,\pm4} + TEM_{0,8}$.

of the two modes behave independently from each other when the mode overlapping coefficient is less than 0.1.

The significant overlapping between the inversion populations usually induces transverse mode competition that may result in a rich set of spatial–temporal dynamics. When two pump sources are used to generate the LG $TEM_{0,2}$ + $TEM_{0,0}$ mode or the LG $TEM_{0,3}$ + $TEM_{0,0}$ mode, precise adjustment of the output mirror is needed to obtain the time average patterns with cylindrical symmetry. Although the time average patterns retain the global symmetry of the system, the complex amplitudes experience complex dynamics due to mode competition. Figures 7(*a*)–(*c*) show the three types of power spectrum and time average patterns in the LG $TEM_{0,2} + TEM_{0,0}$ mode. Near the pump threshold, the pattern in figure 7(*a*) was found to be similar to the stationary 4H (four-hole) configuration described in [14]. Note that the power spectrum for the 4H pattern is almost independent of the acceptance angle of the detector. Slightly above the pump threshold, the intensity transited from the pattern 4H to the rotating pattern TW3 described in [13]. Similar to the unlocked doughnut shown in figure 4(*b*), the appearance of a rather broad peak around 7.5 MHz in the power spectrum of figure 7(*b*) is associated with the rotation. The rotation frequency can be identified from the fact that the rotation frequency nearly disappears when the acceptance angle of the detector is an integral multiple of $\pi/2$. A TW3 rotating pattern has been already observed in a CO_2 laser, as reported in [13]. Even so, the present experiment provides the first observation of the rotating pattern in a solid-state laser and the first observation of the transition from the stationary to the rotating pattern. Further increasing the pump power slightly from the state of the TW3 rotating pattern, the appearance of chaotic generation regimes (figure 7(*c*)) was observed but the time-averaged image was nearly unchanged. Although the appearance of chaotic oscillations is presumably due to the mode coupling, it deserves further investigation.

Finally, we also used the pump sources to excite different high-order LG modes in the double-end-pumping set-up. Similarly, when the pump regions are well separated, the stable multiringed LG modes can be generated. Figures 8(*a*)–(*c*) shows the experimental results for the output beam profiles of multiringed LG modes, measured with the CCD camera. The mode components in figures 8(*a*)–(*c*) are, respectively, $TEM^{*}_{0,\pm1} + TEM_{0,5}$, $TEM_{0,0} + TEM^{*}_{0,\pm3} + TEM_{0,7}$, and $TEM^{*}_{0,\pm2} + TEM^{*}_{0,\pm4} + TEM_{0,8}$.

We have developed a double-end-pumped microchip laser to investigate the superposition and competition of the LG modes. It is found that two LG modes can be directly superposed without significant overlapping between the excited regions. On the other hand, strong competition occurs when the inversion populations have a considerable overlap. In the generation of LG $TEM_{0,2}$ and $TEM_{0,0}$ modes, the transition from the stationary 4H to the rotating pattern TW3 is observed. These observations are consistent with the interesting theoretical predictions in class B lasers. We believe that our experimental method gives a convenient way to investigate the nonlinear dynamics of the LG multi-modes in the class B lasers.

References

[1] Otsuka K, Mandel P and Viktorov E A 1997 Breakup of cw multimode oscillations and low-frequency instability in a microchip solid-state laser by high-density pumping *Phys. Rev.* A **56** 3226–32

[2] Laabs H and Ozygus B 1996 Excitation of Hermite–Gaussian modes in end-pumped solid-state lasers via off-axis pumping *Opt. Laser Technol.* **28** 213–4

[3] Chen Y F, Huang T M, Kao C F, Wang C L and Wang S C 1997 Generation of Hermite Gaussian modes in fiber-coupled laser-diode end-pumped lasers *IEEE J. Quantum Electron.* **33** 1025–31

[4] Dijaloshinski L and Orenstein M 1998 Coupling of concentric semiconductor microring lasers *Opt. Lett.* **23** 364–6

[5] Chen Y F, Lan Y P and Wang S C 2001 Generation of Laguerre–Gaussian modes in fiber-coupled laser-diode end-pumped lasers *Appl. Phys.* B **72** 167–70

[6] Deng Q, Deng H and Deppe D G 1997 Radiation fields from whispering-gallery modes of oxide-confined vertical-cavity surface-emitting lasers *Opt. Lett.* **22** 463–5

[7] Pereira S F, Willemsen M B, Van Exter M P and Woerdman J P 1998 Pinning of daisy modes in optically pumped vertical-cavity surface-emitting lasers *Appl. Phys. Lett.* **73** 2239–41

[8] Haken H 1985 *Light: Laser Light Dynamics* vol 2 (Amsterdam: North-Holland)

[9] Slekys G, Staliunas K and Weiss C O 1995 Motion of phase singularities in a class-B laser *Opt. Commun.* **119** 433–46

[10] Brambilla M *et al* 1994 Dynamical transverse laser patterns. I. Theory *Phys. Rev.* A **49** 1427–51

[11] Coates A B *et al* 1994 Dynamical transverse laser patterns. II. Experiments *Phys. Rev.* A **49** 1452–66

[12] Skryabin D V, Vladimirov A G and Radin A M 1997 Phase and amplitude dynamics of the TEM_{10} and TEM_{01} mode in a class-B laser *Quantum Electron.* **27** 892–6

[13] Boscolo I, Bramati A, Malvezzi M and Prati F 1997 Three-mode rotating pattern in a CO2 laser with high cylindrical symmetry *Phys. Rev.* A **55** 738–43

[14] Prati F, Zucchetti L and Molteni G 1995 Rotating patterns in class-B lasers with cylindrical symmetry *Phys. Rev.* A **51** 4093–108